



Deriving lower bounds on the efficiency of near-degenerate thermal machines via synchronizationTaufiq Murtadho ^{1,2,3}, Juzar Thingna,^{1,2,4,*} and Sai Vinjanampathy ^{5,6,7,†}¹*Center for Theoretical Physics of Complex Systems, Institute for Basic Science, Daejeon 34126, Republic of Korea*²*Basic Science Program, Korea University of Science and Technology, Daejeon 34113, Republic of Korea*³*School of Physical and Mathematical Sciences, Nanyang Technological University, 637371, Singapore*⁴*Department of Physics and Applied Physics, University of Massachusetts, Lowell, Massachusetts 01854, USA*⁵*Department of Physics, Indian Institute of Technology Bombay, Powai, Mumbai 400076, India*⁶*Centre of Excellence in Quantum Information, Computation, Science, and Technology, Indian Institute of Technology Bombay, Powai, Mumbai 400076, India*⁷*Centre for Quantum Technologies, National University of Singapore, 3 Science Drive 2, 117543, Singapore*

(Received 13 January 2023; revised 6 May 2023; accepted 23 June 2023; published 17 July 2023)

We study the relationship between quantum synchronization and the thermodynamic performance of a four-level near-degenerate extension of the Scovil–Schulz–DuBois thermal maser. We show how the existence of interacting coherences can potentially modify the relationship between synchronization and the coherent power output of such a maser. In particular, the cooperation and competition between interacting coherences cause the coherent heat and efficiency to be bounded by the synchronization measure in addition to the well-studied power synchronization bound. Overall, our results highlight the role of quantum synchronization in the working of a thermal machine.

DOI: [10.1103/PhysRevA.108.012205](https://doi.org/10.1103/PhysRevA.108.012205)**I. INTRODUCTION**

Quantum coherence has been a vital resource [1] in quantum thermodynamics and has been a topic of intense research in the recent past [2–5]. The presence of coherence typically boosts the performance metrics of thermal machines such as engines [6], refrigerators [7], and batteries [8–11]. Moreover, coherences, which can be thought of as phases, have also been subject to resource counting studies from an information-theoretic perspective [12]. In the case of nondegenerate systems, that possess diagonal steady states in the absence of driving, such coherences are usually generated using a coherent drive. Such systems do not allow coherences to interact and thus a thorough understanding of the performance of quantum thermal machines with interacting coherences is lacking.

Classically, interacting phases are well studied in coupled Kuramoto models where phase pulling can produce a well-known second-order phase transition involving *cooperative* phase locking called synchronization [13]. Besides this, differences in coupling of the Kuramoto model can lead to *competition* as well, giving rise to a variety of behavior such as antisynchronization and chimera, a phenomenon explored even in the quantum regime [14]. Specifically, in quantum systems, such coupled phase oscillator models arise due to a variety of different reasons, one of them being degeneracies. Recently, for nondegenerate quantum systems coupled to diagonal baths, it was highlighted that synchronization measures fully account for all coherences in the system [15]

and can help explain the performance of quantum thermal machines.

In contrast to coherently driven quantum systems, incoherently driven near-degenerate levels can generate bath-induced coherences. Since the energetic cost of generating coherences is (nearly) zero for making transitions between (near-) degenerate levels, such systems cause the thermodynamic analysis to be decoupled from synchronization. Moreover, the (near) degeneracies cause such coherences to interact with each other and induce cooperation or competition between the different phases.

In an accompanying paper [16], we show that synchronization of driven, dissipative *exactly* degenerate open quantum systems exhibit a crossover from cooperation to competition. In this paper, we highlight that this synchronous behavior aids in the understanding of nanoscale thermal machines. We show that while coherent driving of near-degenerate four-level thermal masers has a tendency to entrain the quantum system to the external drive, coupled coherences exert a simultaneous force that can be either competitive or cooperative. This interplay between cooperation and competition leads to a rich dynamical regime whose implications on the thermal maser are observed in terms of its performance metrics (power, heat, and efficiency) being bounded by the synchronization measure.

In Sec. II below, we begin with a discussion of the near-degenerate four-level thermal maser. Then, we present an analysis of competition and cooperation in four-level thermal masers taking into account near degeneracy and bath-induced coherence in Sec. III. Then, in Secs. IV and V we connect the competition and cooperation to relevant thermodynamic quantities of the thermal machine, specifically its power and

*juzar_thingna@uml.edu

†sai@phy.iitb.ac.in

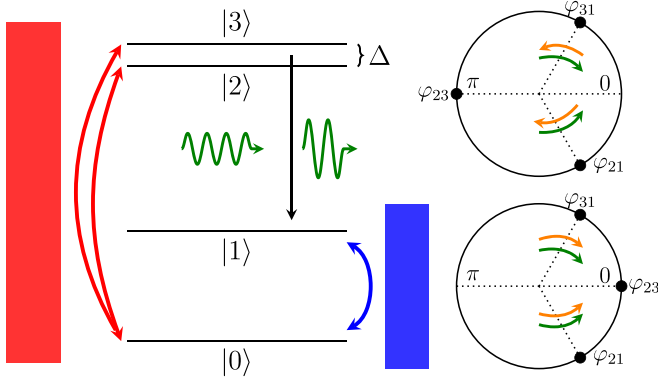


FIG. 1. Schematic of the four-level Scovil–Schulz–DuBois thermal maser. Here, $\Delta \equiv \omega_3 - \omega_2$ is the near-degenerate energy gap and p is the noise-induced coherence strength that arises due to the hot heat bath causing interference between the near-degenerate levels and the ground state (red arrows). The relative phases φ_{ij} between states $|i\rangle$ and $|j\rangle$ are depicted on the circles on the right and the arrows indicate the direction in which the nondegenerate phases (φ_{31} and φ_{21}) move depending on the strength of mutual coupling (orange arrows) and entrainment (green arrows). In the engine (top circle) we observe competition whereas in the refrigerator regime (bottom circle) we find cooperating behavior.

heat current. In [17], the coherent power output of a non-degenerate three-level maser was shown to be related to the measures of synchronization and it was noted in [18] that this relationship does not hold for degenerate systems where there is no energetic cost of generating coherences. Furthermore such degeneracies were related to synchronization blockade recently [19]. We investigate this relationship in detail and connect synchronization to steady-state heat current. The latter is then used to derive the lower bound on the efficiency of near-degenerate thermal machines in the mutual coupling dominant regime. Finally, we summarize our main results in Sec. VI.

II. FOUR-LEVEL THERMAL MASER: NEAR DEGENERACY AND NOISE-INDUCED COHERENCE

We begin with the analysis of a four-level thermal maser that operates under a temperature difference to create a population inversion as depicted in Fig. 1. The original Scovil–Schulz–DuBois thermal maser is a minimal setup composed of three levels and is one of the first models of a thermal heat engine [20], which has been recently extended to four levels [21] and beyond [16,22] to include effects of bath-induced coherence. As a generalization of this, we consider the four-level model consisting of a free Hamiltonian

$$H_0 = \omega_1 |1\rangle \langle 1| + \sum_{j=2}^3 \omega_j |j\rangle \langle j|, \quad (1)$$

with $\omega_3 > \omega_2 > \omega_1 > \omega_0 = 0$. The *near-degenerate* levels (ω_2, ω_3) are spread over a small interval $\Delta \equiv \omega_3 - \omega_2 \ll (\omega_1 - \omega_0)$ and $\Delta \ll (\omega_2 - \omega_1)$. The system is driven out of equilibrium by a hot (temperature T_h) and a cold bath (temperature T_c) as well as an external time-periodic drive of strength λ and frequency $\Omega \approx (\omega_2 - \omega_1)$. The role of the baths is to

establish population inversion between the near-degenerate manifold $\{|2\rangle, |3\rangle\}$ and the first excited state $|1\rangle$. Specifically, when population inversion is achieved, the external drive can easily trigger stimulated emission, thereby producing power, i.e., the system acts as an engine. On the other hand, when the system acts as a refrigerator, there is no population inversion and the system absorbs power from the external drive. When the baths are weakly coupled to the machine working fluid H_0 , the reduced dynamics of the system is governed by a quantum master equation for the reduced density matrix ρ [21] that reads

$$\frac{d\rho}{dt} = -i[H_0 + V(t), \rho] + \mathcal{D}_h[\rho] + \mathcal{D}_c[\rho]. \quad (2)$$

The operator $V(t)$ is a collective drive [16],

$$V(t) = \lambda e^{i\Omega t} \sum_{j=2}^3 |j\rangle \langle 1| + \text{H.c.}, \quad (3)$$

that stimulates transitions between all the near-degenerate energy levels and the first-excited state. The cold-bath dissipator $\mathcal{D}_c[\rho]$ takes the Gorini-Kassakowski-Sudarshan-Lindblad [23,24] form

$$\mathcal{D}_c[\rho] = \sum_{\mu=1}^2 \Gamma_{c_\mu} (2c_\mu \rho c_\mu^\dagger - \{c_\mu^\dagger c_\mu, \rho\}), \quad (4)$$

with jump operators $c_1 = c_2^\dagger = |0\rangle \langle 1|$ and the decay rates satisfying local detailed balance $\Gamma_{c_1} = \gamma_c(1 + n_c)$ and $\Gamma_{c_2} = \gamma_c n_c$. Here, γ_c is the coupling strength squared between the system and the cold bath, and $n_c = (\exp[\omega_1/T_c] - 1)^{-1}$ is the cold-bath distribution with temperature T_c .

The hot-bath dissipator $\mathcal{D}_h[\rho]$ connects the first excited state to the near-degenerate manifold. The near degeneracy causes a breakdown of the secular approximation [25] and results in a Bloch-Redfield form of the dissipator [21,26–29]:

$$\mathcal{D}_h[\rho] = \sum_{\mu=1}^2 \sum_{i,j=2}^3 \Gamma_{\mu}^{ij} [h_{\mu}^i \rho h_{\mu}^{j\dagger}] + \Gamma_{\mu}^{ji} [h_{\mu}^i \rho, h_{\mu}^{j\dagger}]. \quad (5)$$

The operators $h_1^i = h_2^{i\dagger} = |0\rangle \langle i|$ and pairwise decay rates $\Gamma_1^{ij} = P_{ij} \sqrt{\gamma_h^i \gamma_h^j} (1 + n_h^{(j)})$ and $\Gamma_2^{ij} = P_{ij} \sqrt{\gamma_h^i \gamma_h^j} n_h^{(j)}$. Here, γ_h^i denotes the squared coupling strength of the bath that induces transitions between the ground state $|0\rangle$ and the i th state of the near-degenerate manifold $|i\rangle$ ($i = 2, 3$). The mean-bosonic hot-bath distribution $n_h^{(i)} = (\exp[\omega_i/T_h] - 1)^{-1}$ with T_h being the hot bath temperature. In this paper, we will throughout set $\gamma_h^{(2)} = \gamma_h^{(3)} = \gamma_h$ and work with the Redfield form that despite not being positive in all parameter ranges [30,31] provides accurate results when used appropriately in the weak system-bath coupling regime [32,33].

The coefficients P_{ij} are elements of the symmetric *correlation matrix* [34]

$$P_{ij} = \begin{cases} 1 & \text{if } i = j \\ p_{ij} & \text{for } i \neq j \end{cases} \quad (6)$$

where $|p_{ij}| \leq 1$. Since we are focused on a four-level thermal maser, the matrix P is a 2×2 matrix with its off-diagonal elements $|p| \leq 1$. The elements p originate from the dipole-alignment factor [28,29] with $p = \mathbf{d}_2 \cdot \mathbf{d}_3 / |\mathbf{d}_2| |\mathbf{d}_3|$ such that

$\mathbf{d}_i = \langle i|\mathbf{d}|i \rangle$ and \mathbf{d} being the dipole operator. Intuitively, $|p|$ is the strength of quantum interference between thermalization pathways $|0\rangle \leftrightarrow |2\rangle$ and $|0\rangle \leftrightarrow |3\rangle$ while its sign encodes whether the interference is constructive or destructive. Alternatively, the parameter p may be understood as the strength of the noise-induced coherence [21] with $p = 0$ yielding no coherence due to the hot bath and $|p| = 1$ yielding maximum coherence. The above Redfield hot-bath dissipator takes the completely positive Lindblad form [35] when $\Gamma_\mu^{ij} = \Gamma_\mu^{ji} \forall i, j = 2, 3$, which can be satisfied in the exact degenerate limit ($\Delta = 0$ wherein $n_h^{(i)} = n_h$). In this limit, the Kossakowski matrix is proportional to the correlation matrix, and thus positivity can be ensured if the correlation matrix is positive definite, i.e., for $-1 \leq p \leq 1$. When the correlation matrix has a zero eigenvalue ($p = \pm 1$), the dissipator possesses a dark state [36,37] that can lead to multiple steady states [38,39].

The quantum master equation (2) can be transformed to a rotating frame such that any operator $\tilde{O} = \exp[i\tilde{H}t]O\exp[-i\tilde{H}t]$ with

$$\tilde{H} = \frac{\Omega}{2} \sum_{j=2}^3 |j\rangle \langle j| - \frac{\Omega}{2} |1\rangle \langle 1|. \quad (7)$$

The above transformation eliminates the explicit time dependency from the coherent evolution and leaves the dissipators invariant leading to a quantum master equation in the rotating frame,

$$\frac{d\tilde{\rho}}{dt} = -i[H_0 - \tilde{H} + \tilde{V}, \tilde{\rho}] + \mathcal{D}_h[\tilde{\rho}] + \mathcal{D}_c[\tilde{\rho}], \quad (8)$$

with $\tilde{V} = \lambda \sum_{j=2}^3 |j\rangle \langle 1| + \text{H.c.}$ Throughout this paper, we will focus our attention on the four-level thermal maser investigating the effects of near degeneracy Δ and the dipole-alignment factor p (noise-induced coherence strength) on quantum synchronization and the thermodynamic observables of the thermal maser. In particular, unlike [16] we will not explore the effect of several degenerate levels (generalized Scovil–Schulz–DuBois thermal maser) and restrict ourselves to the easily tractable and physically intuitive four-level heat machine.

III. COEXISTENCE OF ENTRAINMENT AND MUTUAL COUPLING IN A NEAR-DEGENERATE THERMAL MASER

The four-level thermal maser forms the minimal model in which entrainment and mutual coupling coexist. In the accompanying paper [16], we show how competition and cooperation manifest in the synchronization measure for degenerate multilevel thermal masers. Depending on the thermodynamic functionality of the maser, the phases compete when the system behaves as an engine and cooperate when it acts as a refrigerator.

The aim of this section is to show that the same phenomena persist even in the presence of noise-induced coherence ($p \neq 0$) and near degeneracy ($\Delta \neq 0$) by analytically and numerically examining the minimal model. We derive the formula for phase-space synchronization measure [40] S_{\max} for the *exactly* degenerate ($\Delta = 0$) four-level maser in presence of noise-induced coherence. This measure not only

captures the strength of steady-state coherences, but also its phase-matching condition [16]. The general SU(D) quantum synchronization measure applicable to D-level systems is presented in [16]. Here, we apply the general result for our specific case of $D = 4$, to obtain

$$S_{\max} = \frac{1}{16\pi^2} \times \begin{cases} |\tilde{\rho}_{12}^{\text{SS}}| + |\tilde{\rho}_{13}^{\text{SS}}| + |\tilde{\rho}_{23}^{\text{SS}}| & \text{if } n_h < n_c \\ |\tilde{\rho}_{12}^{\text{SS}}| + |\tilde{\rho}_{13}^{\text{SS}}| - |\tilde{\rho}_{23}^{\text{SS}}| & \text{if } n_h > n_c \ \& \ k > 2 \\ (1 + \frac{k^2}{2})|\tilde{\rho}_{23}^{\text{SS}}| & \text{if } n_h > n_c \ \& \ k \leq 2, \end{cases} \quad (9)$$

where $k = \gamma_h(1 + n_h)(1 + p)/\lambda$ is the *dissipation-to-driving ratio*. The superscript of $\tilde{\rho}$ denotes the steady state, whose analytical formula can be derived for $\Delta = 0$ and $-1 \leq p \leq 1$ (see Appendix A). The analytical solution for $\tilde{\rho}^{\text{SS}}$ can then be used to derive Eq. (9) by following the recipe in the Supplemental Material of [16]. In fact, Eq. (9) has the same form as the result obtained in [16] with the exception that the dissipation-to-driving ratio k now depends on the noise-induced coherence strength p .

Equation (9) displays cooperation and competition between entrainment and mutual coupling in different thermodynamic regimes. The mutual-coupling (entrainment) contribution is represented by (non)degenerate coherences $|\tilde{\rho}_{ij}^{\text{SS}}|$ ($|\tilde{\rho}_{1j}^{\text{SS}}|$) for $i, j = 2, 3$. In the refrigerator regime ($n_c < n_h$), entrainment and mutual coupling cooperate to increase the overall synchronization of the maser since all steady-state coherences contribute positively to S_{\max} . Meanwhile, in the engine case, we observe competition between coherences for $k > 2$. The competition and cooperation are due to different phase configurations preferred by the two mechanisms, i.e., both prefer in-phase synchronization in the refrigerator case while one prefers in-phase synchronization and the other prefers out-of-phase synchronization in the engine case (see Fig. 2). Moreover, in the engine case for $k < 2$, synchronization is dominated by mutual coupling contribution.

The p dependence of k allows us to explore different synchronization regimes by tuning the strength of noise-induced coherence. For example, in absence of noise-induced coherence ($p = 0$), the deep mutual coupling dominant regime $k \ll 2$ can only be explored in the strong-driving regime $\lambda \gg 2\gamma_h(1 + n_h)$. However, if the driving is strong, one starts to deform the limit cycle and deviate away from the typical synchronization paradigm [13]. Yet, in presence of noise-induced coherence ($p \neq 0$), the deep mutual coupling dominant regime of $k \ll 2$ can be easily explored in presence of total destructive interference ($p \rightarrow -1$).

Figures 2(a) and 2(b) show the quasiprobability phase distribution $S(\varphi_{21}, \varphi_{31})$, where $\varphi_{ij} \equiv \phi_i - \phi_j$ is the relative phase between states $|i\rangle$ and $|j\rangle$. They are computed in the engine regime for $p = 0.5$ and -0.99 . Figure 2(a) shows the regime where entrainment is stronger than mutual coupling so that despite their competition, the phases localize in the rotating frame. On the other hand, Fig. 2(b) shows the deep mutual-coupling dominant regime where entrainment is effectively lost but the relative phase is still fixed. Note that in both figures, the near-degenerate gap is set to be nonzero ($\Delta \neq 0$).

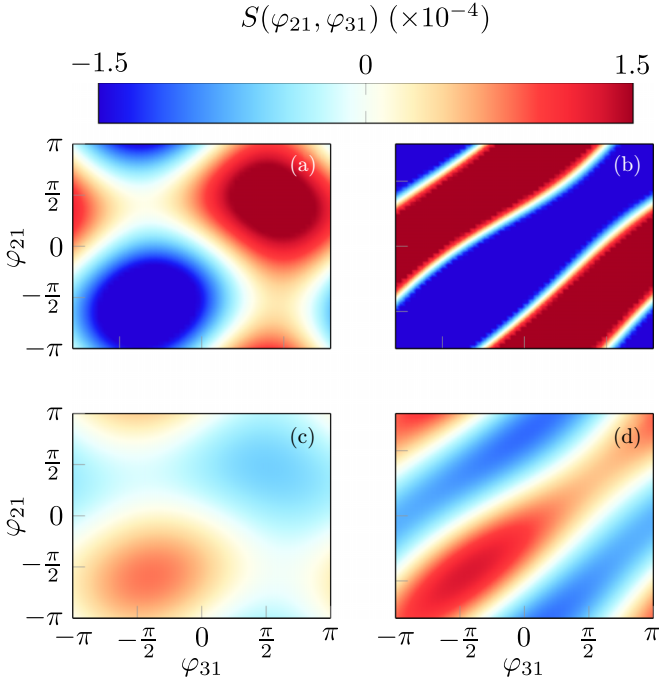


FIG. 2. Quasiprobability phase distribution $S(\varphi_{31}, \varphi_{21})$ in the [(a),(b)] engine ($n_h^{(2)}/n_c = 5$) and [(c),(d)] refrigerator ($n_h^{(2)}/n_c = 0.5$) regime. [(a),(c)] The noise-induced coherence strength $p = 0.5$ with (a) $k = 4.5$ and (c) $k = 3.15$. [(b),(d)] The noise-induced coherence strength $p = -0.99$ with (b) $k = 0.03$ and (d) $k = 0.021$. Above, $\varphi_{ij} \equiv \phi_i - \phi_j$ is the phase difference associated with states $|i\rangle$ and $|j\rangle$. In panels (a) and (c), both φ_{21} and φ_{31} are localized in the rotating frame, indicating entrainment to the external drive. In panels (b) and (d), the phases localize to a ring (on a torus), indicating that only the relative phase $\varphi_{23} = \varphi_{21} - \varphi_{31}$ is fixed. In this regime, synchronization is dominated by mutual coupling. We find that in the engine (refrigerator) regime, the mutual coupling synchronization is out of phase $\varphi_{23} \approx \pm\pi$ (in-phase $\varphi_{23} \approx 0$). Notice that there is a mirror symmetry between the phase distribution in the engine and refrigerator regime, i.e., the maximum (minimum) of $S(\varphi_{21}, \varphi_{31})$ in the engine case is a minimum (maximum) in the refrigerator case. The other model parameters are $\omega_2 = 3\omega_1$, $\Omega = \omega_2 - \omega_1 + \Delta/2$, $\Delta = 0.05\omega_1$, $\gamma_h = \gamma_c = 0.1\omega_1$, $\lambda = 0.05\omega_1$, and $n_c = 0.1$.

IV. THERMODYNAMIC OBSERVABLES

In this section, we will derive the key thermodynamic observables, specifically steady-state power and heat current following the standard recipe for weak-coupling thermodynamics [41]. We follow the standard energy partitioning [42] that defines the internal energy as

$$E = \text{Tr}(\tilde{\rho}H_0). \quad (10)$$

The internal energy here is defined as that of the bare Hamiltonian H_0 and differs from the standard definition that involves the full Hamiltonian [41]. Importantly, such a definition remains the same in all pictures (Schrödinger, Heisenberg, and interaction) and thereby avoids the inconsistencies when one moves from one picture to another. Using the quantum master equation (8), the change in internal energy can be

expressed as

$$\frac{dE}{dt} = -i\text{Tr}([H_0, \tilde{V}]\tilde{\rho}) + \text{Tr}(\mathcal{D}_h[\tilde{\rho}]H_0) + \text{Tr}(\mathcal{D}_c[\tilde{\rho}]H_0). \quad (11)$$

The energy flux is separated into three terms. The first term in (11) is power and the following terms are heat fluxes from the hot and cold bath, respectively [42,43]:

$$P = -i\text{Tr}([H_0, \tilde{V}]\tilde{\rho}) = 2\lambda \sum_{j=2}^3 (\omega_j - \omega_1) \text{Im}(\tilde{\rho}_{1j}), \quad (12)$$

$$\begin{aligned} \dot{Q}_h &= \text{Tr}(\mathcal{D}_h[\tilde{\rho}]H_0) \\ &= 2\gamma_h \left\{ \sum_{j=2}^3 \omega_j [n_h^{(j)} \tilde{\rho}_{00} - (1 + n_h^{(j)}) \tilde{\rho}_{jj}] \right. \\ &\quad \left. - [(1 + n_h^{(2)})\omega_3 + (1 + n_h^{(3)})\omega_2] p \text{Re}(\tilde{\rho}_{23}) \right\}, \quad (13) \end{aligned}$$

$$\dot{Q}_c = \text{Tr}(\mathcal{D}_c[\tilde{\rho}]H_0) = 2\omega_1 \gamma_c [n_c \tilde{\rho}_{00} - (1 + n_c) \tilde{\rho}_{11}]. \quad (14)$$

In the *engine* regime, heat flows from the hot bath to the cold bath and power is produced in the steady state, i.e., $\dot{Q}_h^{\text{SS}} > 0$, $\dot{Q}_c^{\text{SS}} < 0$, $P^{\text{SS}} < 0$. Conversely, in the *refrigerator* regime, heat flows from the cold bath to the hot bath and power is consumed, i.e., $\dot{Q}_h^{\text{SS}} < 0$, $\dot{Q}_c^{\text{SS}} > 0$, $P^{\text{SS}} > 0$.

The heat current to the cold bath \dot{Q}_c depends solely on populations whereas the heat from the hot bath \dot{Q}_h depends on populations and coherences. Intuitively, since the hot bath connects the ground state and the near-degenerate manifold, a finite dipole alignment factor p leads to noise-induced coherence causing the hot heat current to be dependent on both populations and coherences. Thus, the incoherent and coherent contribution to the hot bath's heat current [44,45] can be expressed as

$$\dot{Q}_h^{\text{inc}} = 2\gamma_h \sum_{j=2}^3 \omega_j [n_h^{(j)} \tilde{\rho}_{00} - (1 + n_h^{(j)}) \tilde{\rho}_{jj}], \quad (15)$$

$$\dot{Q}_h^{\text{coh}} = -2\gamma_h [(1 + n_h^{(2)})\omega_3 + (1 + n_h^{(3)})\omega_2] p \text{Re}(\tilde{\rho}_{23}). \quad (16)$$

Note that the coherent heat current is proportional to p which we set to be zero in the accompanying work [16].

The coherent heat either suppresses or enhances the natural inclination of heat flow. For example, in the exactly degenerate ($\Delta = 0$) engine regime, a net heat flow coming from the hot bath to the system creates a population inverted state such that $\dot{Q}_h^{\text{inc,SS}} > 0$. From Eq. (16), we see that the sign of $\dot{Q}_h^{\text{coh,SS}}$ depends on the sign of p [$\cdot \text{Re}(\tilde{\rho}_{23}^{\text{SS}}) < 0$, see Eq. (A19)]. If noise-induced coherence strength $p > 0$ ($p < 0$), then the heat flow is enhanced (suppressed). Similarly, in the exactly degenerate ($\Delta = 0$) refrigerator regime, we observe enhancement or suppression of heat dumped into the hot bath due to either constructive ($p > 0$) or destructive ($p < 0$) interference.

V. CONNECTION BETWEEN THERMODYNAMIC OBSERVABLES AND SYNCHRONIZATION

In general the synchronization measure (S_{max}) and thermodynamic observables (P , \dot{Q}_c , and \dot{Q}_h) are unrelated. However, the power spectrum can be used to demonstrate the frequency-

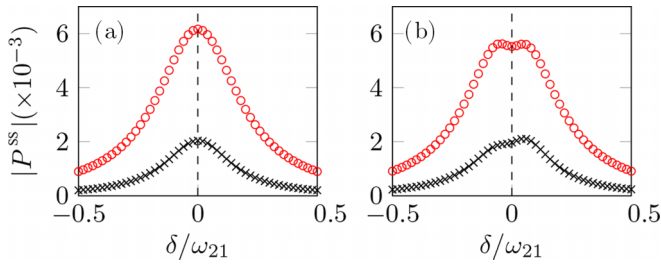


FIG. 3. The power spectrum $|P^{SS}|$ as a function of detuning $\delta = \Omega - (\omega_2 + \omega_3)/2$ for (a) $\Delta = 0.05\omega_1$ and (b) $\Delta = 0.2\omega_1$ in the engine (red circles, $n_h^{(2)}/n_c = 5$) and refrigerator (black crosses, $n_h^{(2)}/n_c$) regimes. When the driving is resonant with the average frequency of the near-degenerate levels the power is maximum ($\delta = 0$) and this behavior persists even close to resonant driving (finite δ) indicating the robustness of the underlying entrainment phenomenon. The noise-induced coherence parameter is $p = 0.8$. Other parameter values are the same as Fig. 2.

locking aspect of synchronization [13,40,46]. In Fig. 3, we plot the absolute value of steady-state power $|P^{SS}|$ as a function of detuning $\delta = \Omega - (\omega_2 + \omega_3)/2$ for different values of near-degenerate energy gap $\Delta = \omega_3 - \omega_2 > 0$. We emphasize that $\delta = 0$ implies the driving frequency is resonant to the *average* frequency of the near-degenerate levels. We demonstrate frequency locking in Fig. 3(a) where the power spectrum peaks at the average frequency. On the other hand, as the degeneracy is further lifted in Fig. 3(b), bimodality emerges in the power spectrum, indicating the loss of frequency entrainment. Note that in Fig. 3(b), the power spectrum in the refrigerator regime is asymmetric with respect to $\delta = 0$. This asymmetry is due to net absorption in which transitions $|1\rangle \rightarrow |2\rangle$ and $|1\rangle \rightarrow |3\rangle$ are both allowed for $\Omega \geq \omega_3 - \omega_1$. Meanwhile, if $\Omega < \omega_3 - \omega_1$, the transition $|1\rangle \rightarrow |3\rangle$ is much less likely to occur due to conservation of energy.

Moreover, in the case of a three-level thermal maser, the steady-state power of the maser is bounded by the synchronization measure [17] [power-synchronization (PS) bound] connecting two seemingly distinct quantities. In this section, we build the general framework of connecting the mathematically abstract notion of synchronization to physical thermodynamic observables for a four-level thermal maser. Despite several efforts analyzing the thermodynamic properties of the four-level thermal maser [21,22,36], there have so far been no connections between the synchronizing ability of such a thermal maser and its thermodynamic observables.

A. Power-synchronization bound

We begin by revisiting the relationship between quantum synchronization and the power of a three-level Scovil–Schulz-DuBois maser, where the steady-state power is bounded by the synchronization measure [17], i.e.,

$$|P^{SS}| \leq \kappa_{3TL} S_{\max}, \quad (17)$$

where $\kappa_{3TL} = 16\pi\lambda(\omega_2 - \omega_1)$ is a proportionality constant for the three-level maser. Inequality (17) is known as the PS bound. The bound above has a different physical interpretation in the engine and refrigerator regimes. In the engine regime,

the PS bound implies that the engine's power is limited by the amount the working substance entrains with the external drive. Whereas, in the refrigerator regime, since power is pumped into the system, the PS bound suggests that there exists a maximum energy cost to ensure that the working substance is entrained to the external drive. In other words, in the engine regime, it can be inferred from the PS bound that synchronization enhances the power output of the engine, whereas in the refrigerator regime, the PS bound suggests that the external power supplied to the machine is utilized to synchronize the working substance.

We now investigate the PS bound for a near-degenerate four-level thermal maser ($D = 4$). Using Eq. (12), the power of the maser can be upper bounded by

$$|P^{SS}| \leq 2\lambda\omega_{31} (|\tilde{\rho}_{12}^{SS}| + |\tilde{\rho}_{13}^{SS}|). \quad (18)$$

The steady-state power $|P^{SS}|$ depends only on those coherences that are influenced *directly* by the external drive, whereas the synchronization measure S_{\max} is linearly dependent on all coherences. While the coherence $|\tilde{\rho}_{23}^{SS}|$ affects the synchronization measure S_{\max} [see Eq. (9)], it does *not* appear in the expression for steady-state power [Eq. (18)]. Due to the additional dependence of $\tilde{\rho}_{23}^{SS}$, we find that the PS bound is respected in the refrigerator case,

$$|P^{SS}| \leq \kappa S_{\max} \quad (n_c > n_h), \quad (19)$$

while being violated in the engine regime ($n_h > n_c$). Above, $\kappa = 32\pi^2\lambda(\omega_3 - \omega_1)$ is a proportionality constant for a four-level maser. The above expression is analytically obtained in the exact degeneracy limit $\Delta = 0$. The violation occurs due to the presence of the near-degenerate levels that induce competition between entrainment and mutual coupling [16]. The origin of the violation can be clearly seen from the expression for S_{\max} [Eq. (9)] that in the engine regime for $k > 2$ reads $S_{\max} \propto |\tilde{\rho}_{12}^{SS}| + |\tilde{\rho}_{13}^{SS}| - |\tilde{\rho}_{23}^{SS}| < |\tilde{\rho}_{12}^{SS}| + |\tilde{\rho}_{23}^{SS}|$. Although Eq. (19) was derived with the assumption $\Delta = 0$ (exact degeneracy), we show in Figs. 4(a) and 4(b) that the violation persists for small nonzero values of Δ where we plot steady-state power to synchronization ratio $|P^{SS}|/(\kappa S_{\max})$ as a function of $n_h^{(2)}/n_c$ and noise-induced coherence strength p . The violation occurs if the ratio exceeds unity.

In Fig. 4(a), we observe that other than a sharp discontinuity near the engine-to-refrigerator transition, $|P^{SS}|/(\kappa_4 S_{\max})$ does not strongly depend on $n_h^{(2)}/n_c$. The discontinuity is due to the discontinuity of $\arg(\tilde{\rho}_{ij}^{SS})$ for $i \neq j$ as shown in Fig. 4(c). On top of being the engine-refrigerator transition, the discontinuity point also marks the transition from cooperation to competition between entrainment and mutual coupling [16]. We find that the PS bound is always satisfied in the refrigerator regime while being violated in the engine regime for small values of Δ . Interestingly, as the near degeneracy is further lifted by increasing Δ , we find that the validity of the PS bound is restored in both the engine and refrigerator regimes.

We also plot $|P^{SS}|/(\kappa S_{\max})$ as a function of noise-induced coherence strength p in both the engine and refrigerator regime [see Fig. 4(b)]. We again observe that the bound is always satisfied in the refrigerator case while it is violated for most values of p in the engine case. As $p \rightarrow -1$, the bound seems to be recovered again. However, this is not guaranteed

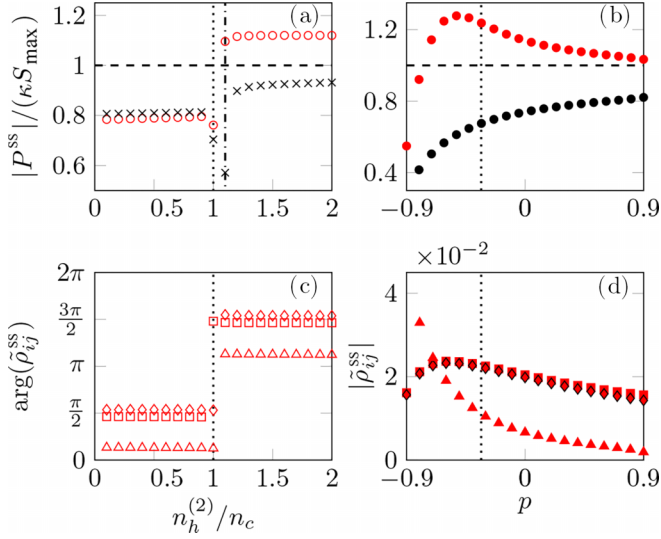


FIG. 4. Steady-state power to synchronization ratio $|P^{SS}|/(\kappa S_{\max})$ with $\kappa = 32\pi^2\lambda(\omega_3 - \omega_1)$ as a function of (a) $n_h^{(2)}/n_c$ and (b) noise-induced coherence parameter p . In panel (a), the near-degenerate energy gap $\Delta = 0.05\omega_1$ (red empty circles), $\Delta = 0.2\omega_1$ (black crosses), and the noise-induced coherence strength $p = 0.5$. In panel (b), the red filled circles are computed in the engine ($n_h^{(2)}/n_c = 5$) regime, and the black filled circles are computed in the refrigerator ($n_h^{(2)}/n_c = 0.5$) regime. The vertical dotted ($\Delta = 0.05\omega_1$) and dash-dotted ($\Delta = 0.2\omega_1$) lines in panel (a) represent the engine-to-refrigerator boundary defined by the change of sign in power. They slightly deviate from the degenerate case ($n_h^{(2)}/n_c = 1$). Meanwhile, the dotted line in panel (b) marks the entrainment-dominant to the mutual-coupling dominant boundary ($k = 2$ or equivalently $p = -1/3$). The power-synchronization bound is satisfied when $|P^{SS}|/(\kappa S_{\max}) \leq 1$ (below the dashed horizontal line) in either panel (a) or panel (b). In panel (c), we plot the argument of steady-state coherence: $\arg(\tilde{\rho}_{12}^{SS})$ (square), $\arg(\tilde{\rho}_{13}^{SS})$ (diamond), and $\arg(\tilde{\rho}_{23}^{SS})$ (triangle) as a function of $n_h^{(2)}/n_c$ with $p = 0.5$. In panel (d), we plot the norm of steady-state coherence: $|\tilde{\rho}_{12}^{SS}|$ (filled squares), $|\tilde{\rho}_{13}^{SS}|$ (filled diamond), and $|\tilde{\rho}_{23}^{SS}|$ (filled triangles) as a function of p in engine regime ($n_h^{(2)}/n_c = 5$). The coherences $|\tilde{\rho}_{12}^{SS}|$ and $|\tilde{\rho}_{13}^{SS}|$ nearly overlap in this panel. Panels (c) and (d) mimic the qualitative behaviors observed in panels (a) and (b), indicating that the coherences are solely responsible for the qualitative behaviors observed in the thermodynamic observables. In both panels (c) and (d), the near-degenerate gap is $\Delta = 0.05\omega_1$. Other parameters' values are the same as Fig. 2.

in general. As $p \rightarrow -1$ or equivalently $k \rightarrow 0$, the expression for S_{\max} only contains degenerate coherence $\tilde{\rho}_{23}^{SS}$ while that of power only contains nondegenerate coherences $\tilde{\rho}_{12}^{SS}$, $\tilde{\rho}_{13}^{SS}$ [see Eq. (9)]. From Fig. 4(d), we find that nondegenerate coherence drops to zero in the limit $p \rightarrow -1$ which means power also drops to zero. However, S_{\max} keeps increasing due to $\tilde{\rho}_{23}^{SS}$. In other words, as $p \rightarrow -1$, synchronization and power start to decouple.

The violation of the power-synchronization bound implies that in degenerate and near-degenerate four-level maser heat engines, more power can be generated than the upper bound set by synchronization. In contrast, in the refrigerator regime ($n_c > n_h$) the PS bound is always satisfied but it is never saturated. This implies that synchronization can be generated

with an energy cost less than the maximum cost imposed by the PS bound.

B. Coherent-heat-synchronization bound

Intuitively, when the working substance of a machine synchronizes it achieves a low entropy state. It is therefore natural to expect that in order to maintain this state the entropy of the bath should increase. Thus, it is expected that synchronization will be coupled to heat. In this subsection, we will solidify this intuition and rigorously show the connections between heat and synchronization, leading to the heat-synchronization (QS) bound.

Specifically, we have seen in Sec. IV that in the presence of noise-induced coherence, the heat contribution from the hot bath can be separated into incoherent and coherent terms. We will now connect the coherent heat current to synchronization by noting the inequality

$$|\dot{Q}_h^{\text{coh,SS}}| \leq 4|p|\gamma_h(1 + n_h^{(2)})\omega_3 \text{Re}(\tilde{\rho}_{23}^{SS}). \quad (20)$$

The above inequality is derived from Eq. (16) by making use of the fact that $\omega_3 \geq \omega_2$ and $n_h^{(2)} \geq n_h^{(3)}$. Note that in contrast to power which is independent of *degenerate coherences* $|\tilde{\rho}_{23}^{SS}|$, the coherent heat current is *only* a function of degenerate coherences. Recall also that synchronization measure S_{\max} is a function of both degenerate and nondegenerate coherences. One may then relate coherent heat current in the steady state with the synchronization measure. In the limit of $\Delta = 0$, we can use Eq. (9) to derive a coherent QS bound

$$|\dot{Q}_h^{\text{coh,SS}}| \leq \alpha S_{\max} \quad (21)$$

where $\alpha = 64\pi^2\gamma_h\omega_3|p|(1 + n_h^{(2)})$ is a proportionality factor. The validity of this bound is trivial in the refrigerator regime where S_{\max} is given by the ℓ_1 norm since $\text{Re}(\tilde{\rho}_{23}^{SS}) \leq |\tilde{\rho}_{23}^{SS}| \leq C_{\ell_1}$. Even in the engine regime, when mutual coupling dominates ($k < 2$), the bound is easily satisfied since $\text{Re}(\tilde{\rho}_{23}^{SS}) \leq |\tilde{\rho}_{23}^{SS}| \leq (1 + k^2/2)|\tilde{\rho}_{23}^{SS}|$. Yet, perhaps more surprisingly, this bound is also valid in the engine entrainment dominant case ($k > 2$). In this regime, since $S_{\max} \propto (2k - 1)|\tilde{\rho}_{23}^{SS}| \geq 3|\tilde{\rho}_{23}^{SS}|$ and $\dot{Q}_h^{\text{coh,SS}} \propto \text{Re}(\tilde{\rho}_{23}^{SS}) \leq |\tilde{\rho}_{23}^{SS}|$, the QS bound is always satisfied. In other words, unlike the PS bound which can be violated in the presence of (near) degeneracy, the QS bound is *always* satisfied at least for the analytically tractable case of $\Delta = 0$.

Although we derived the bound using the exact degeneracy assumption ($\Delta = 0$), we show numerically in Fig. 5 that the bound is still valid for small values of $\Delta \neq 0$. In Figs. 5(a) and 5(b), we plot the coherent heat to synchronization ratio $|\dot{Q}_h^{\text{coh,SS}}|/(\alpha S_{\max})$ for different values of $n_h^{(2)}/n_c$ and noise-induced coherence strength p . We observe that $|\dot{Q}_h^{\text{coh,SS}}|/(\alpha S_{\max})$ does not depend strongly on $n_h^{(2)}/n_c$ except for a discontinuity near the engine-to-refrigerator boundary. Furthermore, we find that the bound is always satisfied and is not strongly dependent on Δ . However, the bound is tight only deep in the mutual coupling regime, e.g., when $p \rightarrow -1$.

C. Lower bound on efficiency and coefficient of performance

Efficiency is one of the most well-known performance metrics for thermal engines. It is defined by $\eta = -P^{SS}/\dot{Q}_h^{SS}$.

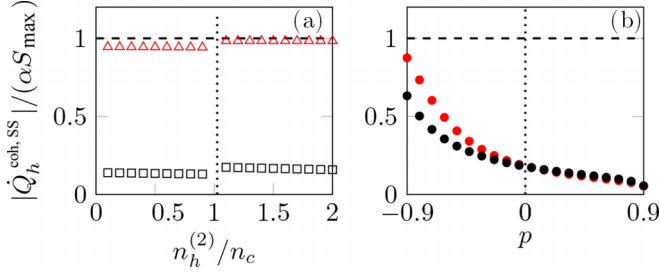


FIG. 5. The coherent heat current to synchronization ratio $\dot{Q}_h^{\text{coh,SS}}/(\alpha S_{\text{max}})$ with $\alpha = 64\pi^2\gamma_h\omega_3|p|(1+n_h^{(2)})$ as a function of (a) $n_h^{(2)}/n_c$ and (b) noise-induced coherence parameter p . The squares in panel (a) are computed for $p = 0.5$ and the triangles are computed for $p = -0.99$. The red filled circles in panel (b) are computed in the engine regime ($n_h^{(2)}/n_c = 5$) and the black filled circles are in the refrigerator regime ($n_h^{(2)}/n_c = 0.5$). All the data points lie below the dashed horizontal line which means the QS bound is always satisfied. The dotted vertical line in panel (a) represents the engine-to-refrigerator boundary and in panel (b) it represents the transition from constructive (positive p) to destructive (negative p) interference. The near-degenerate gap $\Delta = 0.05\omega_1$. Other parameter values are the same as Fig. 2.

Previously, we have demonstrated that both steady-state power P^{SS} and the coherent part of heat current $\dot{Q}_h^{\text{coh,SS}}$ are connected to synchronization measure S_{max} . It is then natural to ask whether efficiency is also connected to synchronization. The efficiency can be computed analytically in the degenerate limit ($\Delta = 0$) and it is given by the standard expression $\eta = 1 - (\omega_1/\omega_2)$ (see Appendix B), which is also obtained for the three-level thermal maser. Thus, the efficiency in the exact degenerate limit depends only on the system's energy scale and it is independent of the synchronization measure S_{max} or any other parameters. However, this is no longer guaranteed in the near-degenerate case ($\Delta \neq 0$), where the steady state is not analytically solvable. In such cases, the efficiency is generally a function of all the parameters of the system, baths, and drive.

It is well known that the efficiency of a heat engine is upper bounded by the Carnot efficiency. Here, we show that synchronization sets a *lower* bound to the efficiency of a near-degenerate thermal maser. We will use the violation of the PS bound and the validity of the QS bound which have been demonstrated for the near-degenerate $\Delta \neq 0$ case in Secs. V A and V B. Below, we state the efficiency-synchronization (ES) bound as

$$\eta \geq \frac{\kappa S_{\text{max}}}{\dot{Q}_h^{\text{inc,SS}} + \alpha S_{\text{max}}}. \quad (22)$$

The above inequality is derived under the assumption that the PS bound is violated $|P^{\text{SS}}| > \kappa S_{\text{max}}$ and the QS bound is respected: $\dot{Q}_h^{\text{inc,SS}} + \dot{Q}_h^{\text{coh,SS}} \leq \dot{Q}_h^{\text{inc,SS}} + |\dot{Q}_h^{\text{coh,SS}}| \leq \dot{Q}_h^{\text{inc,SS}} + \alpha S_{\text{max}}$. Note that the incoherent heat current $\dot{Q}_h^{\text{inc,SS}}$ is only a function of populations [see Eq. (15)] and so it is unrelated to synchronization.

We check the validity of the ES bound Eq. (22) for various parameter values in Figs. 6(a) and 6(b). Similar to the PS and

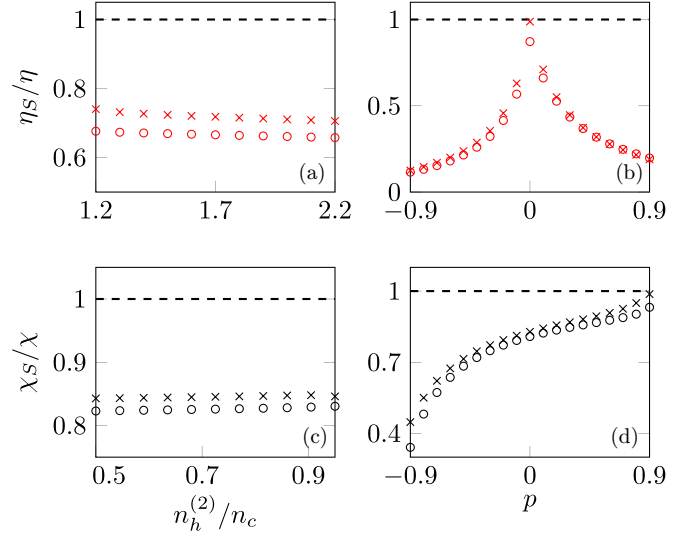


FIG. 6. Synchronization lower-bound engine's efficiency η [(a),(b)] and refrigerator's COP χ [(c),(d)] in a near-degenerate four-level thermal maser. The red (black) data points are computed in the engine (refrigerator) regime. The circles (crosses) are computed with the value of near-degenerate energy gap $\Delta = 0.05\omega_1$ ($\Delta = 0.1\omega_1$). Panels (a) and (b) show efficiency ratio η_S/η [see Eq. (23)] as a function of (a) $n_h^{(2)}/n_c$ and (b) noise-induced coherence parameter p . Similarly, panels (c) and (d) show the COP ratio χ_S/χ [see Eq. (25)] as a function of (c) $n_h^{(2)}/n_c$ and (d) p . In panels (a) and (c) the noise-induced coherence parameter is kept constant at $p = 0.1$. In panels (b) and (d), the baths mean the occupation number ratio is fixed at $n_h^{(2)}/n_c = 2$ and 0.5 , respectively. The bounds (22)–(24) are satisfied if all the data points lie below the dashed horizontal line. Other parameters are the same as in Fig. 2.

QS bound, we find that the ratio η_S/η with

$$\eta_S = \frac{\kappa S_{\text{max}}}{\dot{Q}_h^{\text{inc,SS}} + \alpha S_{\text{max}}} \quad (23)$$

does not strongly depend on the bath's mean occupation number ratio $n_h^{(2)}/n_c$ [Fig. 6(a)]. Instead, it strongly depends on the noise-induced coherence parameter p [Fig. 6(b)]. In the limit when there is no interference effect from the hot bath, i.e., $p \rightarrow 0$, we find that the bound is saturated.

Similarly, the coefficient of performance (COP) in the *exact* degenerate ($\Delta = 0$) refrigerator regime can be analytically computed to be $\chi = \omega_1/(\omega_2 - \omega_1)$ (see Appendix B). In the near-degenerate ($\Delta \neq 0$) case, the COP is lower bounded by the inverse of synchronization measure S_{max} :

$$\chi = \frac{\dot{Q}_c^{\text{SS}}}{P^{\text{SS}}} \geq \frac{\dot{Q}_c^{\text{SS}}}{\kappa S_{\text{max}}}. \quad (24)$$

The lower bound is valid because the consumed power is always upper bounded by S_{max} in the refrigerator regime [see Eq. (19)]. We also note that \dot{Q}_c^{SS} is only a function of populations [see Eq. (14)] and hence is unrelated to the synchronization.

We check the validity of the bound Eq. (24) for various values of parameters in Figs. 6(c) and 6(d). Similar to the ES

TABLE I. The result of this paper, where the check mark indicates that the bound is satisfied whereas the cross means the bound is violated.

	Engine	Refrigerator
PS bound	×	✓
QS bound	✓	✓
ES bound	✓	✓

bound, we find that the ratio χ_S/χ , with

$$\chi_S = \frac{\dot{Q}_c^{SS}}{\kappa S_{\max}}, \quad (25)$$

does not strongly depend on the bath's mean occupation number ratio $n_h^{(2)}/n_c$ [Fig. 6(c)], but depends strongly on the noise-induced coherence parameter p [Fig. 6(d)]. However, different from the ES bound, the bound (24) is saturated in the limit $p \rightarrow 1$, i.e., when the hot bath causes constructive interference.

VI. SUMMARY AND DISCUSSION

There is intense debate regarding the optimal design of quantum thermal machines. Almost all design paradigms assume the systems are well modeled by Markovian master equations and furthermore pursue coherence from an information-theoretic resource cost point of view or a nonequilibrium cost point of view. While such analyses are definitely sufficient for nondegenerate systems, secular approximation begins to fail to describe near-degenerate systems interacting with a bath. Furthermore, interacting coherences can be well understood under the paradigm of coupled oscillator models, an analysis that has tremendously benefited classical dynamical systems.

In this paper, we argue fundamentally that such a coupled oscillator model is indispensable to understanding the subtle dynamics of interacting coherences, which arise due to a variety of situations like those described in this paper. We developed the synchronization dynamics for a four-level atom coupled to two baths, generalizing the canonical thermal maser analysis by Scovil and Schulz-DuBois. We show that coherences interact with each other in two distinct qualitative ways. The first of these is a cooperative phase-locking phenomenon understood as entrainment dynamics of coherences being driven by an external field. Such entrainment dynamics and their contribution to the performance of a thermal maser were discussed earlier [17]. In this paper, we add to this entrainment dynamics and highlight the competition between coherences that can arise due to the bath coupling in our model. This coexistence of cooperation and competition gives rise to a richer tapestry of dynamics, uncoupling the power output from the thermal maser from the synchronization measure.

In the presence of noise-induced coherence, in addition to the power-synchronization bound, we also find that coherent heat is bounded by synchronization measure, showing that synchronization not only influences the useful work [47,48] but can also bound the wasteful heat (see Table I). The lower

bound of the COP is included in the refrigerator column of the ES bound for compactness. Unlike the standard upper bounds like the Carnot efficiency, our analysis shows that efficiency can be *lower* bounded in presence of quantum synchronization. In other words, a quantum synchronous working substance can boost the efficiency of the machine. Even though our analysis was limited to a four-level thermal maser, it would be an interesting future avenue to investigate other coupled oscillator models for interacting coherences to inform the future designs of quantum thermal machines.

ACKNOWLEDGMENTS

This research was supported by the Institute for Basic Science in South Korea (Grant No. IBS-R024-Y2). S.V. acknowledges support from the Government of India under DST-QUEST Grant No. DST/ICPS/QuST/Theme-4/2019. The authors would like to thank V. Singh for the useful discussions.

APPENDIX A: STEADY STATE OF A FOUR-LEVEL THERMAL MASER WITH INTERFERENCE

The quantum master equation (8) can be expanded into a series of linear first-order differential equations for each density-matrix element. We divide the elements into three groups: populations (ρ_{ii} with $i = 0, \dots, 3$), nondegenerate coherences (ρ_{12} and ρ_{13}), and degenerate coherences (ρ_{23}). In the following derivation, we have ignored the coherences ρ_{0i} with $i = 1, 2, 3$ since their dynamics are decoupled from other density-matrix elements and they decay to zero in the steady state.

We restrict ourselves to the exact degenerate case scenario with $\Delta = 0$ and $n_h^{(i)} = n_h$ and obtain the equations for the populations, namely,

$$\frac{d\tilde{\rho}_{11}}{dt} = i\lambda \sum_{j=2}^3 (\tilde{\rho}_{1j} - \tilde{\rho}_{j1}) - 2\xi_c \tilde{\rho}_{11} + 2\gamma_c n_c \tilde{\rho}_{00}, \quad (A1)$$

$$\begin{aligned} \frac{d\tilde{\rho}_{22}}{dt} = & -i\lambda(\tilde{\rho}_{12} - \tilde{\rho}_{21}) - \xi_h p(\tilde{\rho}_{23} + \tilde{\rho}_{32}) - 2\xi_h \tilde{\rho}_{22} \\ & + 2\gamma_h n_h \tilde{\rho}_{00}, \end{aligned} \quad (A2)$$

$$\begin{aligned} \frac{d\tilde{\rho}_{33}}{dt} = & -i\lambda(\tilde{\rho}_{13} - \tilde{\rho}_{31}) - \xi_h p(\tilde{\rho}_{23} + \tilde{\rho}_{32}) - 2\xi_h \tilde{\rho}_{33} \\ & + 2\gamma_h n_h \tilde{\rho}_{00}. \end{aligned} \quad (A3)$$

Above we have introduced $\xi_x = \gamma_x(1 + n_x)$ with $x = c, h$ to simplify our notation. The equations for the nondegenerate and degenerate coherences read

$$\begin{aligned} \frac{d\tilde{\rho}_{12}}{dt} = & i(\omega_2 - \omega_1 - \Omega)\tilde{\rho}_{12} - (\xi_c + \xi_h)\tilde{\rho}_{12} \\ & - \xi_h p\tilde{\rho}_{13} + i\lambda(\tilde{\rho}_{11} - \tilde{\rho}_{22} - \tilde{\rho}_{32}), \end{aligned} \quad (A4)$$

$$\begin{aligned} \frac{d\tilde{\rho}_{13}}{dt} = & i(\omega_2 - \omega_1 + \Delta - \Omega)\tilde{\rho}_{13} - (\xi_c + \xi_h)\tilde{\rho}_{13} \\ & - \xi_h p\tilde{\rho}_{12} + i\lambda(\tilde{\rho}_{11} - \tilde{\rho}_{33} - \tilde{\rho}_{23}), \end{aligned} \quad (A5)$$

$$\begin{aligned} \frac{d\tilde{\rho}_{23}}{dt} = & -i\Delta\tilde{\rho}_{23} - 2\xi_h \tilde{\rho}_{23} - i\lambda(\tilde{\rho}_{13} - \tilde{\rho}_{21}) \\ & + 2\gamma_h n_h p \rho_{00} - \xi_h p(\tilde{\rho}_{22} + \tilde{\rho}_{33}). \end{aligned} \quad (A6)$$

To find an analytical steady-state ($d\tilde{\rho}_{ij}/dt = 0 \forall i, j$) solution, we further restrict ourselves to the resonant drive $\Omega = \omega_2 - \omega_1$ and degenerate ($\Delta = 0$) limit. Using Eqs. (A4) and (A5) and splitting them into their real and imaginary parts we obtain

$$\text{Re}(\tilde{\rho}_{12}^{\text{SS}}) + \text{Re}(\tilde{\rho}_{13}^{\text{SS}}) = 0, \quad (\text{A7})$$

$$[\xi_c + \xi_h(1-p)]\text{Re}(\tilde{\rho}_{12}^{\text{SS}}) + i\lambda \text{Im}(\tilde{\rho}_{23}^{\text{SS}}) = 0. \quad (\text{A8})$$

Furthermore, using Eq. (A7) and computing the imaginary part of Eq. (A6) we obtain

$$2\xi_h \text{Im}(\tilde{\rho}_{23}^{\text{SS}}) + i\lambda \text{Re}(\tilde{\rho}_{12}^{\text{SS}}) = 0. \quad (\text{A9})$$

Note that both Eqs. (A8) and (A9) are linear, involving the same density-matrix elements. Therefore, combining these two equations yields

$$\text{Re}(\tilde{\rho}_{12}^{\text{SS}}) = \text{Re}(\tilde{\rho}_{13}^{\text{SS}}) = \text{Im}(\tilde{\rho}_{23}^{\text{SS}}) = 0, \quad (\text{A10})$$

i.e., the steady-state (non)degenerate coherences are real (imaginary). Further simplification can be sought by subtracting the imaginary part of Eq. (A4) from Eq. (A5) to yield

$$[\xi_c + \xi_h(1-p)][\text{Im}(\tilde{\rho}_{12}^{\text{SS}}) - \text{Im}(\tilde{\rho}_{13}^{\text{SS}})] + i\lambda(\tilde{\rho}_{22}^{\text{SS}} - \tilde{\rho}_{33}^{\text{SS}}) = 0. \quad (\text{A11})$$

The equation above connects the difference between nondegenerate coherences and the population difference between the degenerate states. We can find another linearly independent equation by computing the population differences between degenerate states using Eqs. (A2) and (A3), i.e.,

$$i\lambda[\text{Im}(\tilde{\rho}_{12}^{\text{SS}}) - \text{Im}(\tilde{\rho}_{13}^{\text{SS}})] + \xi_h(\tilde{\rho}_{22}^{\text{SS}} - \tilde{\rho}_{33}^{\text{SS}}) = 0. \quad (\text{A12})$$

Combining the above two equations gives

$$\text{Im}(\tilde{\rho}_{12}^{\text{SS}}) = \text{Im}(\tilde{\rho}_{13}^{\text{SS}}) \quad \text{and} \quad \tilde{\rho}_{22}^{\text{SS}} = \tilde{\rho}_{33}^{\text{SS}}. \quad (\text{A13})$$

Thus, the population and the coherences associated with the degenerate states are equal. This makes intuitive sense because we are working in the exact degenerate limit. Using the constraints derived thus far together with a trace-preserving condition $\tilde{\rho}_{00}^{\text{SS}} = 1 - \tilde{\rho}_{11}^{\text{SS}} - \tilde{\rho}_{22}^{\text{SS}} - \tilde{\rho}_{33}^{\text{SS}}$, the problem is reduced to four independent variables: $\tilde{\rho}_{11}^{\text{SS}}$, $\tilde{\rho}_{22}^{\text{SS}}$, $\tilde{\rho}_{12}^{\text{SS}}$, and $\tilde{\rho}_{23}^{\text{SS}}$. The corresponding four equations to solve for these variables can be derived from Eqs. (A1)–(A6) and they can be expressed as

$$\begin{aligned} 2i\lambda\tilde{\rho}_{12}^{\text{SS}} - \xi_c\tilde{\rho}_{11}^{\text{SS}} + \gamma_cn_c(1 - \tilde{\rho}_{11}^{\text{SS}} - 2\tilde{\rho}_{22}^{\text{SS}}) &= 0, \\ [\xi_c + \xi_h(1+p)]\tilde{\rho}_{12}^{\text{SS}} - i\lambda(\tilde{\rho}_{11}^{\text{SS}} - \tilde{\rho}_{22}^{\text{SS}} - \tilde{\rho}_{23}^{\text{SS}}) &= 0, \\ i\lambda\tilde{\rho}_{12}^{\text{SS}} + \xi_h p\tilde{\rho}_{23}^{\text{SS}} + \xi_h\tilde{\rho}_{22}^{\text{SS}} - \gamma_h n_h(1 - \tilde{\rho}_{11}^{\text{SS}} - 2\tilde{\rho}_{22}^{\text{SS}}) &= 0, \\ i\lambda\tilde{\rho}_{12}^{\text{SS}} + \xi_h\tilde{\rho}_{23}^{\text{SS}} + \xi_h p\tilde{\rho}_{22}^{\text{SS}} - \gamma_h p n_h(1 - \tilde{\rho}_{11}^{\text{SS}} - 2\tilde{\rho}_{22}^{\text{SS}}) &= 0. \end{aligned} \quad (\text{A14})$$

Solving the above linear system of equations for the four-independent steady-state density-matrix elements we first obtain the ratio between nondegenerate and degenerate coherence:

$$\frac{\tilde{\rho}_{12}^{\text{SS}}}{\tilde{\rho}_{23}^{\text{SS}}} = i \frac{\gamma_h(1+n_h)(1+p)}{\lambda}. \quad (\text{A15})$$

The norm of the above quantity is the *dissipation-to-driving ratio* k [defined below Eq. (9)]. It is a crucial quantity to determine the synchronization regime of the system (*entrainment dominant* or *mutual-coupling dominant*) and in observing competition between these mechanisms in the engine regime [see Eq. (9)]. Solving for the populations gives us

$$\begin{aligned} \tilde{\rho}_{11}^{\text{SS}} &= \frac{(1+n_h)\{2\lambda^2[n_c\gamma_c + \gamma_h(1+p)n_h] + \xi_h(1+p)\gamma_cn_c[\xi_c + \xi_h(1+p)]\}}{F(n_h, n_c, \gamma_h, \gamma_c, \lambda, p)}, \\ \tilde{\rho}_{22}^{\text{SS}} = \tilde{\rho}_{33}^{\text{SS}} &= \frac{\lambda^2[n_h + n_c + 2n_h n_c + 2\xi_h n_h(1+p)] + \xi_c \xi_h(1+p)n_h[\xi_c + \xi_h(1+p)]}{F(n_h, n_c, \gamma_h, \gamma_c, \lambda, p)}, \end{aligned} \quad (\text{A16})$$

with the denominator

$$\begin{aligned} F(n_h, n_c, \gamma_h, \gamma_c, \lambda, p) &= 2\lambda^2[\gamma_c(1+3n_c+2n_h+4n_h n_c) + \xi_h(1+p)(1+4n_h)] \\ &\quad + \gamma_c \xi_h(1+p)(1+3n_h+2n_c+4n_h n_c)[\xi_c + \xi_h(1+p)]. \end{aligned} \quad (\text{A17})$$

On the other hand, using the population results, the steady-state *coherences* read

$$\tilde{\rho}_{12}^{\text{SS}} = \tilde{\rho}_{13}^{\text{SS}} = i \frac{\lambda\gamma_c \xi_h(1+p)(n_c - n_h)}{F(n_h, n_c, \gamma_h, \gamma_c, \lambda, p)}, \quad (\text{A18})$$

$$\tilde{\rho}_{23}^{\text{SS}} = \frac{\lambda^2\gamma_c(n_c - n_h)}{F(n_h, n_c, \gamma_h, \gamma_c, \lambda, p)}. \quad (\text{A19})$$

These steady-state coherences are the important quantities in deriving the synchronization measure S_{max} [see (9)]. The

derivation of S_{max} from the steady-state coherences has been explained in detail in our accompanying paper [16].

APPENDIX B: THERMODYNAMIC OBSERVABLES IN STEADY STATE

In Appendix A, we derived the expressions for the steady state of a degenerate four-level thermal maser with interference ($p \neq 0$). We can use those formulas to express thermodynamic observables such as power and heat current in the steady state [see (12)–(14)]:

$$P^{\text{SS}} = -\frac{2\lambda^2\gamma_c \xi_h(\omega_2 - \omega_1)(1+p)(n_h - n_c)}{F(n_h, n_c, \gamma_h, \gamma_c, \lambda, p)}, \quad (\text{B1})$$

$$\dot{Q}_c^{\text{SS}} = -\frac{2\lambda^2\gamma_c \xi_h \omega_1(1+p)(n_h - n_c)}{F(n_h, n_c, \gamma_h, \gamma_c, \lambda, p)}, \quad (\text{B2})$$

$$\dot{Q}_h^{\text{inc,SS}} = \frac{2\lambda^2\omega_2\gamma_c\xi_h(n_h - n_c)}{F(n_h, n_c, \gamma_h, \gamma_c, \lambda, p)}, \quad (\text{B3})$$

$$\dot{Q}_h^{\text{coh,SS}} = \frac{2p\lambda^2\omega_2\gamma_c\xi_h(n_h - n_c)}{F(n_h, n_c, \gamma_h, \gamma_c, \lambda, p)}, \quad (\text{B4})$$

where the total heat current from the hot bath is the total of coherent and incoherent contribution $\dot{Q}_h^{\text{SS}} = \dot{Q}_h^{\text{inc,SS}} + \dot{Q}_h^{\text{coh,SS}}$. It is interesting to note that $\dot{Q}_h^{\text{coh,SS}}/\dot{Q}_h^{\text{inc,SS}} = p$. This relation gives a thermodynamic meaning to noise-induced coherence parameter p as the ratio between coherent and incoherent heat current in the steady state. It also implies the suppression or enhancement of heat flow due to coherence is fully determined by the sign of p . When there is destructive interference ($p < 0$), the direction of coherent heat flow is opposite to the incoherent one (suppression) whereas for constructive interference ($p > 0$) they are in the same direction (enhancement).

Recall that the direction of power and heat flow determines whether the system operates as an engine or refrigerator. In the engine regime, heat flows from the hot bath to the cold bath, and power is produced ($\dot{Q}_h^{\text{SS}} > 0$, $\dot{Q}_c^{\text{SS}} < 0$, $P^{\text{SS}} < 0$). Conversely, in the refrigerator regime, heat flows from the cold bath to the hot bath, and power is consumed ($\dot{Q}_h^{\text{SS}} < 0$, $\dot{Q}_c^{\text{SS}} > 0$, $P^{\text{SS}} > 0$). Equations (B1)–(B4) imply that in the exact

degenerate case ($\Delta = 0$), the engine-to-refrigerator transition is fully determined by the bath's bosonic mean-occupation number. Specifically, $n_h > n_c$ ($n_h < n_c$) implies the maser is functioning as an engine (refrigerator).

In the engine regime ($n_h > n_c$), the efficiency η is calculated as

$$\eta = -\frac{P^{\text{SS}}}{\dot{Q}_h^{\text{SS}}} = 1 - \frac{\omega_1}{\omega_2} \leq \eta_C, \quad (\text{B5})$$

where $\eta_C = 1 - T_c/T_h$ is the Carnot efficiency ($T_{c,h}$ are the temperatures of the cold and hot bath, respectively). The Carnot bound can be obtained by writing $\omega_1 = T_c \ln[(1 + n_c)/n_c]$ and $\omega_2 = T_h \ln[(1 + n_h)/n_h]$.

Meanwhile, in the refrigerator regime ($n_h < n_c$), we calculate the COP:

$$\chi = \frac{\dot{Q}_c^{\text{SS}}}{P^{\text{SS}}} = \frac{\omega_1}{\omega_2 - \omega_1}. \quad (\text{B6})$$

We emphasize that the simple forms of efficiency and COP derived in Eqs. (B5) and (B6) are only valid in the degenerate limit ($\Delta = 0$). In the main text, we lift the degeneracy and show that the efficiency and the COP are lower bounded by synchronization measure S_{max} .

-
- [1] A. Streltsov, G. Adesso, and M. B. Plenio, Colloquium: Quantum coherence as a resource, *Rev. Mod. Phys.* **89**, 041003 (2017).
- [2] F. Binder, L. A. Correa, C. Gogolin, J. Anders, and G. Adesso, *Thermodynamics in the Quantum Regime* (Springer, New York, 2018).
- [3] J. Goold, M. Huber, A. Riera, L. Del Rio, and P. Skrzypczyk, The role of quantum information in thermodynamics: A topical review, *J. Phys. A* **49**, 143001 (2016).
- [4] J. Millen and A. Xuereb, Perspective on quantum thermodynamics, *New J. Phys.* **18**, 011002 (2016).
- [5] S. Vinjanampathy and J. Anders, Quantum thermodynamics, *Contemp. Phys.* **57**, 545 (2016).
- [6] J. Son, P. Talkner, and J. Thingna, Monitoring quantum otto engines, *PRX Quantum* **2**, 040328 (2021).
- [7] R. Kosloff and A. Levy, Quantum heat engines and refrigerators: Continuous devices, *Annu. Rev. Phys. Chem.* **65**, 365 (2014).
- [8] F. Campaioli, F. A. Pollock, F. C. Binder, L. Céleri, J. Goold, S. Vinjanampathy, and K. Modi, Enhancing the Charging Power of Quantum Batteries, *Phys. Rev. Lett.* **118**, 150601 (2017).
- [9] D. Rossini, G. M. Andolina, D. Rosa, M. Carrega, and M. Polini, Quantum Advantage in the Charging Process of Sachdev-Ye-Kitaev Batteries, *Phys. Rev. Lett.* **125**, 236402 (2020).
- [10] S. Julià-Farré, T. Salamon, A. Riera, M. N. Bera, and M. Lewenstein, Bounds on the capacity and power of quantum batteries, *Phys. Rev. Res.* **2**, 023113 (2020).
- [11] J. Son, P. Talkner, and J. Thingna, Charging quantum batteries via Otto machines: Influence of monitoring, *Phys. Rev. A* **106**, 052202 (2022).
- [12] J. P. Santos, L. C. Céleri, G. T. Landi, and M. Paternostro, The role of quantum coherence in non-equilibrium entropy production, *npj Quantum Inf.* **5**, 23 (2019).
- [13] A. Pikovsky, M. Rosenblum, and J. Kurths, *Synchronization: A Universal Concept in Nonlinear Science* (Cambridge University Press, Cambridge, 2002).
- [14] V. M. Bastidas, I. Omelchenko, A. Zakharova, E. Schöll, and T. Brandes, Quantum signatures of chimera states, *Phys. Rev. E* **92**, 062924 (2015).
- [15] N. Jaseem, M. Hajdušek, P. Solanki, L.-C. Kwek, R. Fazio, and S. Vinjanampathy, Generalized measure of quantum synchronization, *Phys. Rev. Res.* **2**, 043287 (2020).
- [16] T. Murtadho, S. Vinjanampathy, and J. Thingna, Cooperation and Competition in Synchronous Open Quantum Systems, *Phys. Rev. Lett.* **131**, 030401 (2023).
- [17] N. Jaseem, M. Hajdušek, V. Vedral, R. Fazio, L.-C. Kwek, and S. Vinjanampathy, Quantum synchronization in nanoscale heat engines, *Phys. Rev. E* **101**, 020201(R) (2020).
- [18] P. Solanki, N. Jaseem, M. Hajdušek, and S. Vinjanampathy, Role of coherence and degeneracies in quantum synchronization, *Phys. Rev. A* **105**, L020401 (2022).
- [19] P. Solanki, F. M. Mehdi, M. Hajdušek, and S. Vinjanampathy, Symmetries and synchronization blockade, [arXiv:2212.09388](https://arxiv.org/abs/2212.09388) [Phys. Rev. A (to be published)].
- [20] H. E. D. Scovil and E. O. Schulz-DuBois, Three-Level Masers as Heat Engines, *Phys. Rev. Lett.* **2**, 262 (1959).
- [21] K. E. Dorfman, D. Xu, and J. Cao, Efficiency at maximum power of a laser quantum heat engine enhanced by noise-induced coherence, *Phys. Rev. E* **97**, 042120 (2018).
- [22] W. Niedenzu, D. Gelbwaser-Klimovsky, and G. Kurizki, Performance limits of multilevel and multipartite quantum heat machines, *Phys. Rev. E* **92**, 042123 (2015).

- [23] V. Gorini, A. Kossakowski, and E. C. G. Sudarshan, Completely positive dynamical semigroups of N level systems, *J. Math. Phys.* **17**, 821 (1976).
- [24] G. Lindblad, On the generators of quantum dynamical semigroups, *Commun. Math. Phys.* **48**, 119 (1976).
- [25] H.-P. Breuer and F. Petruccione, *The Theory of Open Quantum Systems* (Oxford University, New York, 2002).
- [26] F. Bloch, Generalized theory of relaxation, *Phys. Rev.* **105**, 1206 (1957).
- [27] A. G. Redfield, On the theory of relaxation processes, *IBM J. Res. Dev.* **1**, 19 (1957).
- [28] G. S. Agarwal and S. Menon, Quantum interferences and the question of thermodynamic equilibrium, *Phys. Rev. A* **63**, 023818 (2001).
- [29] T. V. Tscherbul and P. Brumer, Partial secular Bloch-Redfield master equation for incoherent excitation of multilevel quantum systems, *J. Chem. Phys.* **142**, 104107 (2015).
- [30] J. Thingna, J.-S. Wang, and P. Hänggi, Generalized Gibbs state with modified Redfield solution: Exact agreement up to second order, *J. Chem. Phys.* **136**, 194110 (2012).
- [31] J. Thingna, J.-S. Wang, and P. Hänggi, Reduced density matrix for nonequilibrium steady states: A modified Redfield solution approach, *Phys. Rev. E* **88**, 052127 (2013).
- [32] R. Hartmann and W. T. Strunz, Accuracy assessment of perturbative master equations: Embracing nonpositivity, *Phys. Rev. A* **101**, 012103 (2020).
- [33] T. Becker, A. Schnell, and J. Thingna, Canonically Consistent Quantum Master Equation, *Phys. Rev. Lett.* **129**, 200403 (2022).
- [34] G. Marsaglia and I. Olkin, Generating correlation matrices, *SIAM J. Sci. Stat. Comput.* **5**, 470 (1984).
- [35] By “Lindblad” we refer to the general Lindblad form $d\rho/dt = -i[H, \rho] + \sum_{i,j} K_{ij}(2A_i\rho A_j^\dagger - \{A_j^\dagger A_i, \rho\})$ where $A_i \equiv h_i$ are the jump operators and K_{ij} is the positive Kossakowski matrix.
- [36] D. Gelbwaser-Klimovsky, W. Niedenzu, P. Brumer, and G. Kurizki, Power enhancement of heat engines via correlated thermalization in a three-level “working fluid,” *Sci. Rep.* **5**, 14413 (2015).
- [37] J. Thingna, D. Manzano, and J. Cao, Dynamical signatures of molecular symmetries in nonequilibrium quantum transport, *Sci. Rep.* **6**, 28027 (2016).
- [38] J. Thingna, D. Manzano, and J. Cao, Magnetic field induced symmetry breaking in nonequilibrium quantum networks, *New J. Phys.* **22**, 083026 (2020).
- [39] J. Thingna and D. Manzano, Degenerated Liouvillians and steady-state reduced density matrices, *Chaos* **31**, 073114 (2021).
- [40] S. Walter, A. Nunnenkamp, and C. Bruder, Quantum Synchronization of a Driven Self-Sustained Oscillator, *Phys. Rev. Lett.* **112**, 094102 (2014).
- [41] R. Alicki, The quantum open system as a model of the heat engine, *J. Phys. A* **12**, L103 (1979).
- [42] E. Boukobza and D. J. Tannor, Thermodynamics of bipartite systems: Application to light-matter interactions, *Phys. Rev. A* **74**, 063823 (2006).
- [43] E. Boukobza and D. J. Tannor, Three-Level Systems as Amplifiers and Attenuators: A Thermodynamic Analysis, *Phys. Rev. Lett.* **98**, 240601 (2007).
- [44] C. L. Latune, I. Sinayskiy, and F. Petruccione, Apparent temperature: Demystifying the relation between quantum coherence, correlations, and heat flows, *Quantum Sci. Technol.* **4**, 025005 (2019).
- [45] C. L. Latune, I. Sinayskiy, and F. Petruccione, Energetic and entropic effects of bath-induced coherences, *Phys. Rev. A* **99**, 052105 (2019).
- [46] S. Sonar, M. Hajdušek, M. Mukherjee, R. Fazio, V. Vedral, S. Vinjanampathy, and L.-C. Kwek, Squeezing Enhances Quantum Synchronization, *Phys. Rev. Lett.* **120**, 163601 (2018).
- [47] T. Herpich, J. Thingna, and M. Esposito, Collective Power: Minimal Model for Thermodynamics of Nonequilibrium Phase Transitions, *Phys. Rev. X* **8**, 031056 (2018).
- [48] J.-W. Ryu, A. Lazarescu, R. Marathe, and J. Thingna, Stochastic thermodynamics of inertial-like Stuart-Landau dimer, *New J. Phys.* **23**, 105005 (2021).